Journal of Molecular Catalysis A: Chemical 318 (2010) 21–29

Contents lists available at ScienceDirect

Journal of Molecular Catalysis A: Chemical

journal homepage: www.elsevier.com/locate/molcata

The role of impregnation medium on the activity of ceria-supported cobalt catalysts for ethanol steam reforming

Hua Song, Umit S. Ozkan*

Department of Chemical & Biomolecular Engineering, The Ohio State University, Columbus, OH 43210, USA

ARTICLE INFO

Article history:
Received 2 May 2009
Received in revised form 22 October 2009
Accepted 4 November 2009
Available online 12 November 2009

Keywords:
Cobalt catalyst
Ceria
Ethanol steam reforming
Impregnation medium
DRIFTS
Raman
XPS

ABSTRACT

The effect of impregnation medium on the activity of Co/CeO_2 catalysts in ethanol steam reforming was investigated using various characterization techniques including temperature programmed calcination, temperature programmed reduction, X-ray diffraction, laser Raman spectroscopy, X-ray photoelectron spectroscopy, and diffuse reflectance infrared fourier transform spectroscopy. The steady-state reaction experiments showed that catalysts that were prepared in an organic medium (e.g., ethanol) during impregnation gave higher H_2 yields than those prepared in aqueous media. Characterization results showed the presence of oxygenated carbonaceous species left on the surface from the impregnation step. These species, which were stable through oxidation and reduction pre-treatment steps, may possibly contribute to the activity, selectivity and stability of the catalysts by keeping the Co particles segregated and by blocking the sites for side reactions.

1. Introduction

Hydrogen continues to hold promise as an important energy carrier for the future, with its high gravimetric energy density, its low impact on the environment, and its potential as a fuel for more efficient energy conversion devices such as fuel cells. With increasing demand for hydrogen, producing it from renewable sources, such as bio-derived liquids, is also gaining increased importance. Bio-ethanol offers a promising starting material for hydrogen due to its low toxicity, its ease of handling and its availability from many different renewable sources, ranging from sugar cane to algae. Hydrogen produced from a bio-source has the potential to recycle the CO_2 produced during its production through photosynthesis during plant growth. Finally, producing hydrogen through steam reforming of bio-derived liquids such as bio-ethanol lends itself well to a distributed production strategy.

Recent years have seen a significant increase in the number of studies on ethanol steam reforming (ESR). Catalysts utilized are mainly Ni, Cu, Co and noble metals, such as Rh, Ru, Re, Pd, Ir and Pt [1–4], which are reviewed by Haryanto et al. [5] and Vaidya and Rodrigues [6]. Although supported noble metal catalysts have been shown to have excellent performance during ESR in 500–600 °C range and high space velocities [7–9], the high and widely fluctuating cost of these metals limits their wide applications. As a less expensive alternative, cobalt-based catalysts have been reported to have superior ethanol steam reforming performance due to their high activity for C–C bond cleavage at temperatures as low as 350–400 °C [10–12]. At these temperatures, researchers have reported good selectivity to CO_2 and H_2 with CH_4 being the only by-product.

Various metal oxides, most of which have been reported by Llorca et al. [12], have been used as support materials for Co in order to provide a high surface area as well as good thermal stability leading to better cobalt dispersion even at higher temperatures. Although cobalt catalysts supported on these oxides showed comparable activity, the product distribution was significantly different indicating that these selected supports actively participated in the ESR reaction. Among the various supports, ceria offers increased resistance to coking due to its high oxygen storage capacity (OSC) and oxygen mobility, as shown in many other reactions that involve an oxidation step such as CO oxidation, water–gas shift, and steam reforming of methane [13–15]. Increased oxygen mobility promotes gasification and oxidation of carbon deposits on the surface, hence improving stability, which was demonstrated in our previous studies [16].

In addition to the support effects mentioned above, several other promotional effects have been extensively investigated aiming to enhance the catalytic activity as well as stability during ESR. For instance, the addition of alkaline metals (e.g., Li, Na, and K) has been shown to improve the catalytic performance [17–19]. In addition,

* Corresponding author. Tel.: +1 614 292 6623; fax: +1 614 292 3769.
E-mail address: Ozkan.1@osu.edu (U.S. Ozkan).

1381-1169/$ – see front matter © 2009 Elsevier B.V. All rights reserved.
doi:10.1016/j.molcata.2009.11.003

use of different cobalt precursors [20–22], different preparation techniques, and synthesis/pre-treatment parameters [23–25] have been shown to have a significant impact on the catalytic performance. One conclusion emerging from various studies is that the catalytic activity is directly related to cobalt dispersion [26,27].

There have been reports in the literature, showing an effect of the impregnation medium used in the preparation of supported Co catalysts for Fischer-Tropsch reaction [28]. In this paper, as a continuation of our previous work [16,23,29], we examine the role of the impregnation medium on the activity of Co-based catalysts for ethanol steam reforming. The supported catalysts were prepared by incipient wetness impregnation (IWI) and characterized through temperature programmed calcination (TPC), temperature programmed reduction (TPR), *in situ* X-ray diffraction (XRD), *in situ* laser Raman spectroscopy (LRS), X-ray photoelectron spectroscopy (XPS), and diffuse reflectance infrared fourier transform spectroscopy (DRIFTS). The results from characterization studies were used in explaining the activity differences observed for catalysts prepared in different media.

2. Experimental

2.1. Catalysts preparation

Supported cobalt catalysts with 10% weight loading were prepared in air by IWI technique. Cerium (IV) oxide (nanopowder, <25 nm, Aldrich) was calcined at 550 °C for 4 h, resulting in a support with a surface area and pore volume of 71 m^2/g and 0.34 cm^3/g, respectively. Cobalt (II) nitrate hexahydrate (Aldrich 99.999%), which was used as the cobalt precursor, was dissolved in either ethanol or deionized water and then impregnated on the previously calcined support. After repeated impregnation and drying steps (overnight at approximately 95 °C) as many times as required by the pore volume of the CeO_2 support, the as-prepared samples were calcined at 450 °C under air for 3 h and stored for later use. In the nomenclature used in this paper, the letter in parenthesis following the catalyst formulation represents the impregnation medium, i.e., A for aqueous (DI water) and E for ethanol.

2.2. Catalysts characterization

Cobalt dispersion was determined through a H_2 chemisorption technique using a Micromeritics ASAP 2010 Chemisorption system. Prior to adsorption measurements, calcined samples were pretreated at 450 °C and then reduced *in situ* under 5%H_2/He at 400 °C for 2 h followed by evacuation to 1.33–0.67 KPa and cooling down to 50 °C to maximize activated chemisorption while minimizing H_2 spillover [30]. The adsorption isotherms were measured at equilibrium pressures between 6.67 and 66.7 kPa. The first adsorption isotherm was established by measuring the amount of H_2 adsorbed as a function of pressure. After completing the first adsorption isotherm, the system was evacuated for 1 h at 1.33–0.67 kPa. Then a second adsorption isotherm was obtained. The amount of probe molecule chemisorbed was calculated by taking the difference between the two isothermal adsorption amounts. Metallic surface area was determined by assuming a one-to-one stoichiometry between Co and atomic hydrogen and a cross-sectional area of 0.0662 nm^2 for a Co atom.

The calcination process was investigated through TPC experiment. The sample was placed between two layers of quartz wool in a stainless steel reactor which was placed in the center of a temperature programmable furnace. A constant air flow rate was maintained over the sample throughout the process and the reactor outlet stream was monitored by a Cirrus Mass Spectrometer (MKS Instruments, 1–300 amu).

H_2 TPR experiments were performed using a laboratory flow system equipped with a thermal conductivity detector (TCD). Samples of 50 mg were loaded into a U-tube and then subjected to an oxidative cleaning step at the samples' calcination temperature in air, followed by cooling to room temperature under helium. TPR experiments were subsequently performed under 5%H_2/N_2 (30 ml/min) with a heating rate of 10 °C/min. The exit gas from the reactor was sent to a column filled with silica gel for trapping water before being sent to the TCD for analysis.

XRD profiles were collected from 20° to 90° at a step width of 0.0144° using Bruker D8 advance X-ray diffractometer. *In situ* XRD was also performed during calcination process under air (30 ml/min) and reduction process under 5%H_2/N_2 (30 ml/min) using a linear heating rate of 0.3 °C/min and holding at different preset temperatures for a given time for stabilizing and data collection. The XRD patterns used for particle size estimation at various stages of the catalyst life-time were collected from 20° to 90° at a step width of 0.002° using Rigaku Ultima III X-ray diffractometer equipped with a CuKα source (λ = 1.5406 Å).

Raman spectra were taken with a LabRAM HR-800 spectrometric analyzer integrated with OLYMPUS BX41 microscope (50× magnification) and CCD detector. The *in situ* calcination experiment was performed under air (30 ml/min) using an "operando cell". The sample was first heated to various temperatures and cooled down to room temperature where the spectra were taken using an argon ion laser (514.5 nm, operated at 3 mW). A similar procedure was followed while performing *in situ* reduction experiment under 5%H_2/He (30 ml/min).

XPS analysis was performed using an AXIS His, 165 Spectrometer manufactured by Kratos Analytical with a monochromatized Al X-ray source. 2.3 V voltage was chosen to make the charge balance. The sample was pressed into a stainless steel cup before loading into the instrument. The survey scan was performed to identify all the elements within the sample, followed by regional scans for Co 2p, C 1s, O 1s, Ce 3d orbitals in order to achieve the high resolution for these elements of interest. A controlled-atmosphere transfer chamber was used for transferring the samples to the XPS instrument in order to prevent the reduced samples from being re-oxidized again. For quantification of the surface and near surface concentrations of elements, the instrument-dependent atomic sensitivity factors were used.

DRIFTS was performed with a Thermo NICOLET 6700 FTIR spectrometer equipped with a liquid-nitrogen-cooled MCT detector and a KBr beam splitter. The experiments were performed using a Smart collector DRIFT environmental chamber with ZnSe windows. For room-temperature spectra, following a cleaning step under He at 450 °C for 30 min to remove impurities from sample surface that might have adsorbed during storage, the chamber was cooled down to room temperature under He and sample spectra were then collected. As background, the spectrum taken over the sample impregnated in aqueous media was used.

2.3. Activity tests

The catalytic activity tests were performed in a tubular quartz reactor (4 mm internal diameter). The catalyst was placed between two layers of quartz wool. The aqueous ethanol solution (EtOH:H_2O = 1:10 at molar ratio) was delivered into the evaporator by an isocratic pump (Eldex MicroPro). The feed vapors generated were carried by helium and sent into the reactor after being combined with nitrogen, which was used as internal standard. The delivery lines were heated with heat tapes to prevent condensation.

All catalysts were first pretreated at 450 °C for 30 min under He and then reduced *in situ* at 400 °C for 2 h under 5%H_2/He. Subsequently the catalytic performances were tested in the temperature range of 300–500 °C, in 50 °C increments. The catalyst was held at

Table 1
Product distribution during steady-state reaction over 10%Co/CeO_2(A) and 10%Co/CeO_2(E) at various temperatures: H_2O:EtOH = 10:1 (molar ratio), WHSV = 0.48 gEtOH/g Cat/h, GHSV = ~20,000 h^{-1}, and C_{EtOH} = 2%.

Products[a]	300 °C		350 °C		400 °C		450 °C		500 °C	
	(A)	(E)	(A)	(E)	(A)	(E)	(A)	(E)	(A)	(E)
% yield										
H_2	10.9	42.4	32.9	83.3	64.7	88.9	71.4	89.4	74.9	91.4
% selectivity										
CO_2	5.6	55.1	17.4	85.6	29.9	91.2	35.0	90.4	59.4	88.5
CO	4.1	2.3	7.5	2.9	4.4	2.8	5.5	4.6	5.8	6.6
CH_4	3.5	3.2	5.2	8.4	2.9	6.0	2.7	4.9	10.9	4.9
C_2H_4	0	0	0.0	0.0	0.0	0.0	1.2	0.0	2.7	0.0
C_2H_6	0	0	0.0	0.0	0.0	0.0	0.0	0.0	0.7	0.0
CH_3COCH_3	6.0	3.5	37.0	3.1	62.8	0.0	55.6	0.0	20.6	0.0
CH_3CHO	80.7	35.9	29.5	0.0	0.0	0.0	0.0	0.0	0.0	0.0
$(C_2H_5)_2O$	0	0	3.4	0.0	0.0	0.0	0.0	0.0	0.0	0.0

[a] The values reported in the table are defined in Section 2.3.

each temperature for at least 2 h. At the end of the catalytic test, the flow of EtOH + H_2O was stopped and the catalyst was cooled under a He stream.

The analysis of the reactants and all the reaction products was carried out online by gas chromatography (Shimadzu Scientific 2010). Analysis was done using two different detectors and the separation was achieved using two different sample injection loops/valves and two analysis lines: the first line consisted of a Carboxen column and a 5-Å molecular sieve column connected in series in a column isolation scheme. This combined column arrangement was used in conjunction with a pulse discharge helium ionization detector (PDHID). The second line was a separate 30 m-long Q-Plot column used with a methanizer and a flame ionization detector (FID) to allow detection of CO as low as 10 ppm. Helium was used as the carrier gas for both of the analysis lines. All the carbon-containing products could be separated by the Q-Plot column and detected by FID. PDHID can detect all the products in the stream, including CO, CO_2, and H_2. Response factors for all products were obtained and the system was calibrated with appropriate standards before each catalytic test.

The H_2 yield, selectivity and yield of carbon-containing products, and ethanol conversion were defined as follows:

$$H_2\ \text{yield}\,\% = \frac{\text{moles of } H_2 \text{ produced}}{6 \times (\text{moles of ethanol fed})} \times 100$$

$$\text{Yield of C-containing product, } i\,\% = \frac{\#\text{C} \times (\text{moles of } i \text{ produced})}{2 \times (\text{moles of ethanol fed})} \times 100$$

$$\text{Selectivity of C-containing product } i\ 6 = \frac{\#\text{C} \times (\text{moles of } i \text{ produced})}{2 \times (\text{moles of ethanol converted})}$$

$$\text{EtOH Conv.}\,\% = \frac{\text{moles of ethanol converted}}{\text{moles of ethanol fed}} \times 100$$

The turnover frequency (TOF) reported in the paper is calculated based on the ethanol conversion rate and hydrogen production, respectively, divided by the total metallic cobalt active sites exposed on the surface of the catalysts in the reactor, which was determined from H_2 chemisorption experiment described above.

3. Results and discussion

3.1. Catalytic performance comparison

Table 1 shows the H_2 yields and the selectivities for C-containing products. At every temperature tested, the catalysts prepared in an organic medium, give higher H_2 yields and CO_2 selectivity while selectivities to CO and CH_4 are lower. Another important aspect of the product distribution comparison is that Co/CeO_2(E) catalyst does not have any liquid products left in the product stream above 350 °C, with CH_4 and CO being the only other products besides CO_2 and H_2. Catalyst prepared in an aqueous media, on the other hand, continues to have significant levels of acetone in the product stream even at higher temperatures. In addition, although their amount is relatively small, other undesirable by-products such as diethyl ether, ethylene, and ethane are also observed over Co/CeO_2(A) at various temperatures. Formation of C_2 hydrocarbons suggests hydration steps that might lead to coke formation.

When TOFs for the (E) and (A) catalysts are compared, it is seen that ethanol conversion TOFs are comparable for the two catalysts (0.006 and 0.007 s^{-1} at 300 °C, respectively). TOFs for H_2 formation, however, show a much higher activity for Co/CeO_2(E), with a value more than twice that of the (A) catalysts (0.011 and 0.024 s^{-1} at 300 °C, respectively), indicating a higher ability for C–C bond cleavage and for complete oxidation of C in the ethanol molecule.

The ethanol-impregnated catalyst was kept on stream for 40 h to examine its stability. Fig. 1 shows the ethanol conversion and product yields during the run at 350 °C. For the duration of the experiment, the catalyst has shown no sign of deactivation, maintaining an ethanol conversion of 85%, a H_2 yield of ~82% and a CO_2 yield of ~70%. The yield of all other products remained low, below 8%. When a similar time-on-stream experiment was

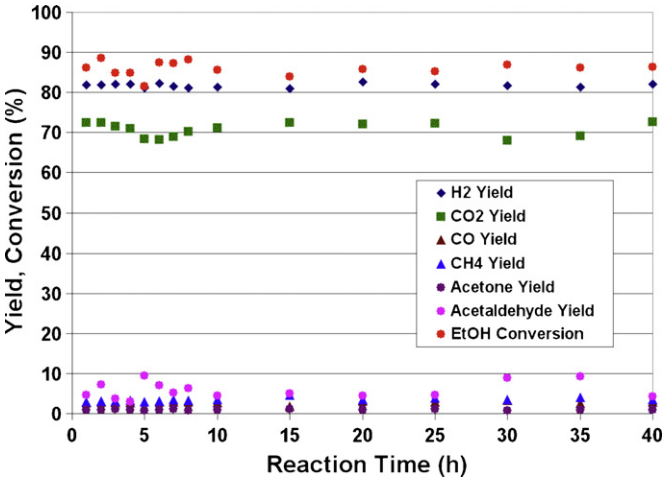

Fig. 1. Time-on-stream behavior of 10 Co/CeO_2(E) catalyst at 350 °C. Reaction conditions: H_2O:EtOH = 10:1 (molar ratio), WHSV = 0.48 g EtOH/g Cat/h, GHSV = ~20,000 h^{-1}, and C_{EtOH} = 2%.

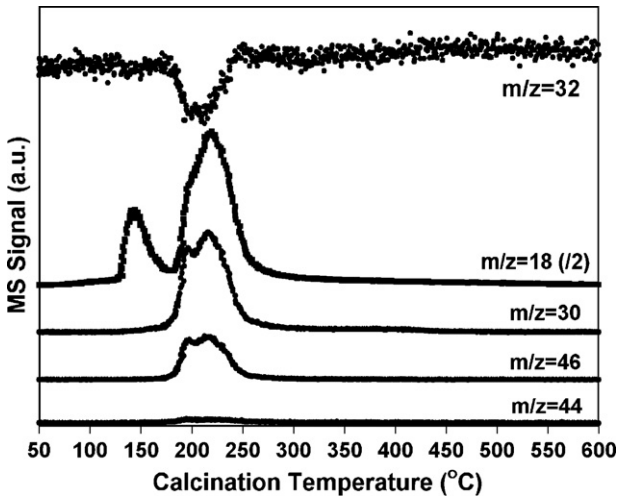

Fig. 2. Elution of gas phase species over Co/CeO_2(E) during the calcination process.

performed over the Co/CeO_2(A) catalyst, rapid deactivation was observed starting within 15 h (data not shown). Once activity loss started, the main products were hydrocarbons, signaling dehydration reaction becoming important. Poor carbon balance during this period suggested coking on the surface, which was verified by post-deactivation examination of the spent catalyst.

3.2. Characterization

Catalysts prepared in the two different impregnation media were characterized using various techniques, in an effort to understand the possible surface and structural characteristics that might contribute to the differences in performance.

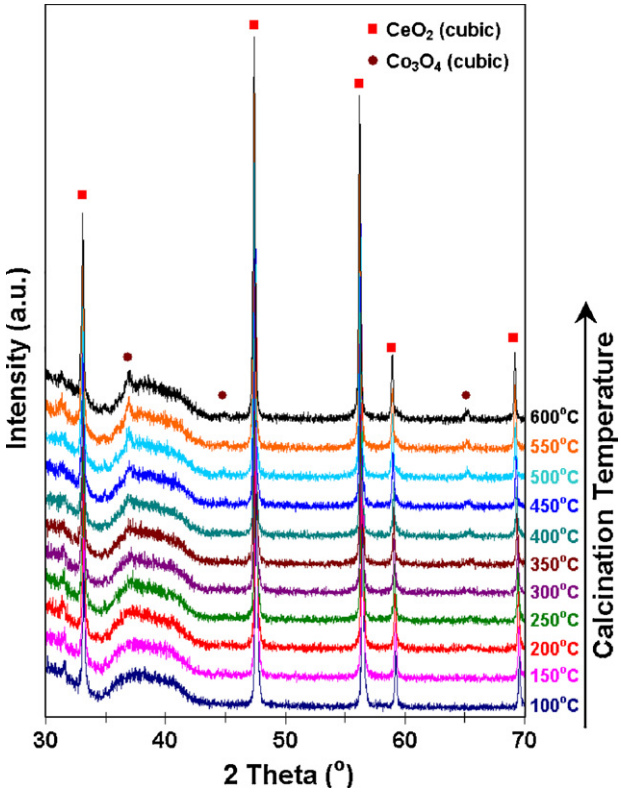

Fig. 3. *In situ* XRD patterns of Co/CeO_2(E) taken during the calcination process.

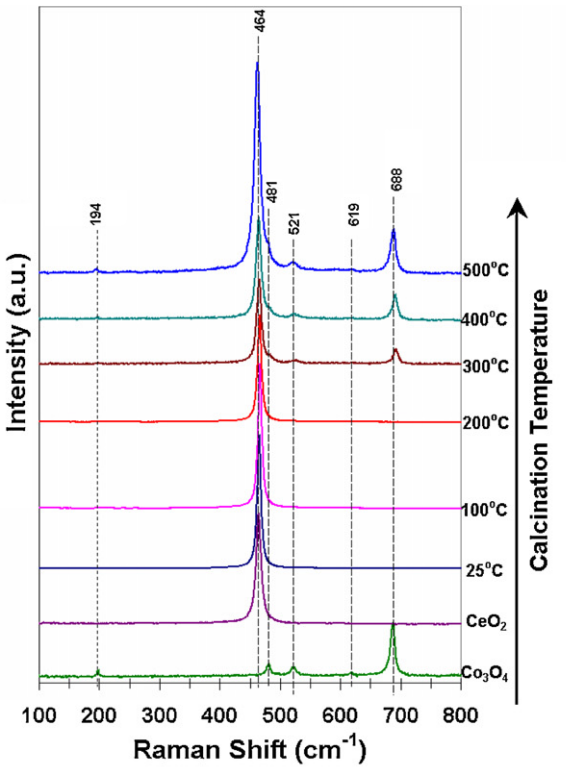

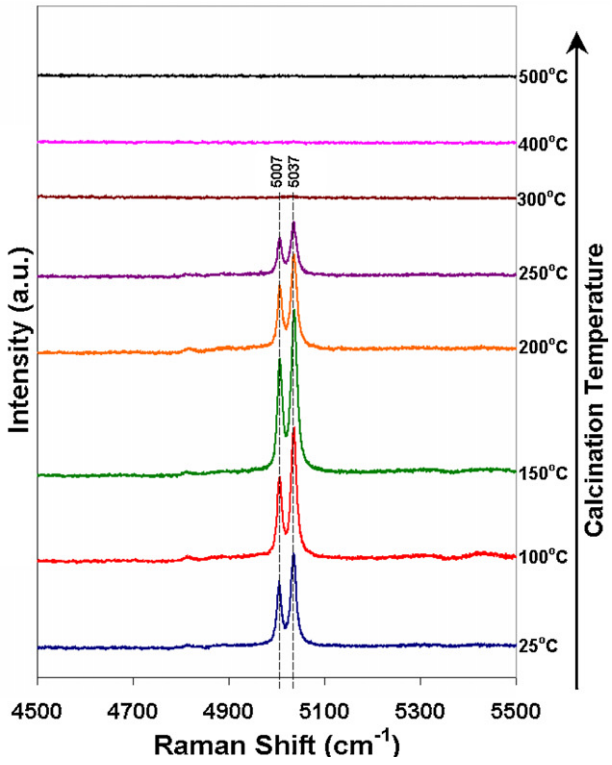

Fig. 4. *In situ* Raman spectra collected over/CeO_2(E) during the calcination process.

Fig. 2 shows the gas phase species eluting from the Co/CeO_2(E) sample during the calcination process. Water is seen to form at two distinct temperatures. The low-temperature feature indicates the release of the crystal water present in the cobalt precursor. The larger peak at higher temperature might be derived from the OH groups in the sample formed from the ethanol impregnation during sample preparation. The combination of 30 and 46 ion fragments

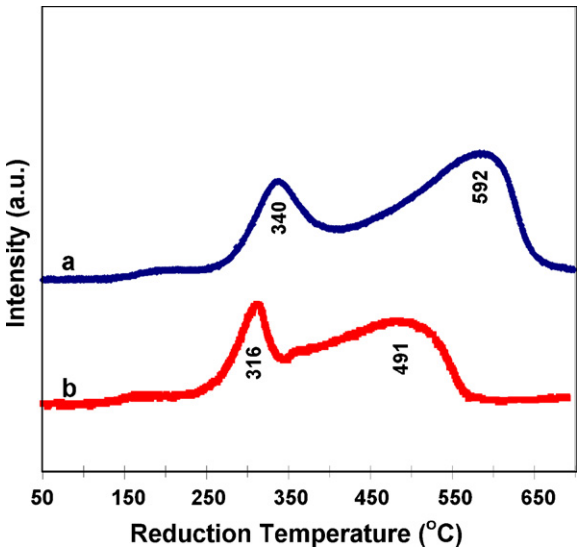

Fig. 5. H_2 TPR profiles of (a) Co/CeO_2(A) and (b) Co/CeO_2(E).

reveals the production of NO_x from the cobalt nitrate oxidative decomposition, which is accompanied by the corresponding oxygen consumption. No carbon-containing gas products are detected. The gas phase species eluting from the sample prepared in the aqueous media exhibited similar features of H_2O and NO_x species (profiles not shown).

The calcination process of the catalyst impregnated in an ethanol medium was further examined using the XRD technique. Although there is a broad feature from 35° to 45° due to the fluorescence of Co, the signal can still be discriminated from the background. As shown in Fig. 3, the cubic CeO_2 support is visible at each temperature. However, the evolution of the cobalt oxide can seen be with increasing calcination temperature. When the temperature is above 300 °C, the diffraction peaks corresponding to cubic Co_3O_4 begin to appear. The gradual increase of the Co_3O_4 peak along with increasing calcination temperature implies the growth of Co_3O_4 particles at higher temperatures.

The calcination process over the Co/CeO_2(E) sample was also examined by laser Raman spectroscopy. Fig. 4 shows the *in situ* Raman spectra collected during calcination. The low wavenumber region (100–800 cm^{-1}) shows the formation of Co_3O_4 and higher region (4500–5500 cm^{-1}) shows the decomposition of cobalt nitrate, left behind from the impregnation step. Although cobalt nitrate has a major Raman band centered around 1050 cm^{-1}, when impregnated onto CeO_2, its signal is masked due to the highly Raman active nature of the support. Therefore, the evolution of the nitrate phase was followed in the high wavenumber region. As seen in Fig. 4, CeO_2 peak is observed throughout the process without changing, Co_3O_4 begins to appear when the temperature is above 300 °C. The gradual increase of the Co_3O_4 peak along with increasing calcination temperature implies the growth of Co_3O_4 particles at higher temperature. The doublet shown in high wavenumber region shows the cobalt nitrate decomposition which is completed when the temperature is above 300 °C which coincides with the formation of Co_3O_4. The catalyst precursor for the Co/CeO_2(A) showed a similar evolution through the calcination process (data not shown).

The reduction behaviors of the Co/CeO_2(E) and Co/CeO_2(A) are studied using the TPR technique and the results are shown in Fig. 5. Two peaks are observed and identified as Co_3O_4–CoO and CoO–Co reduction features, using CuO to calibrate H_2 consumption and Co_3O_4 as a standard reference. When the reduction profiles for the two catalysts were compared, the sample synthesized in the organic media showed noticeably better reducibility, which correlates well with ESR activity [23]. Neither surface nor bulk reduction of CeO_2 occurs within the reduction temperature range investigated.

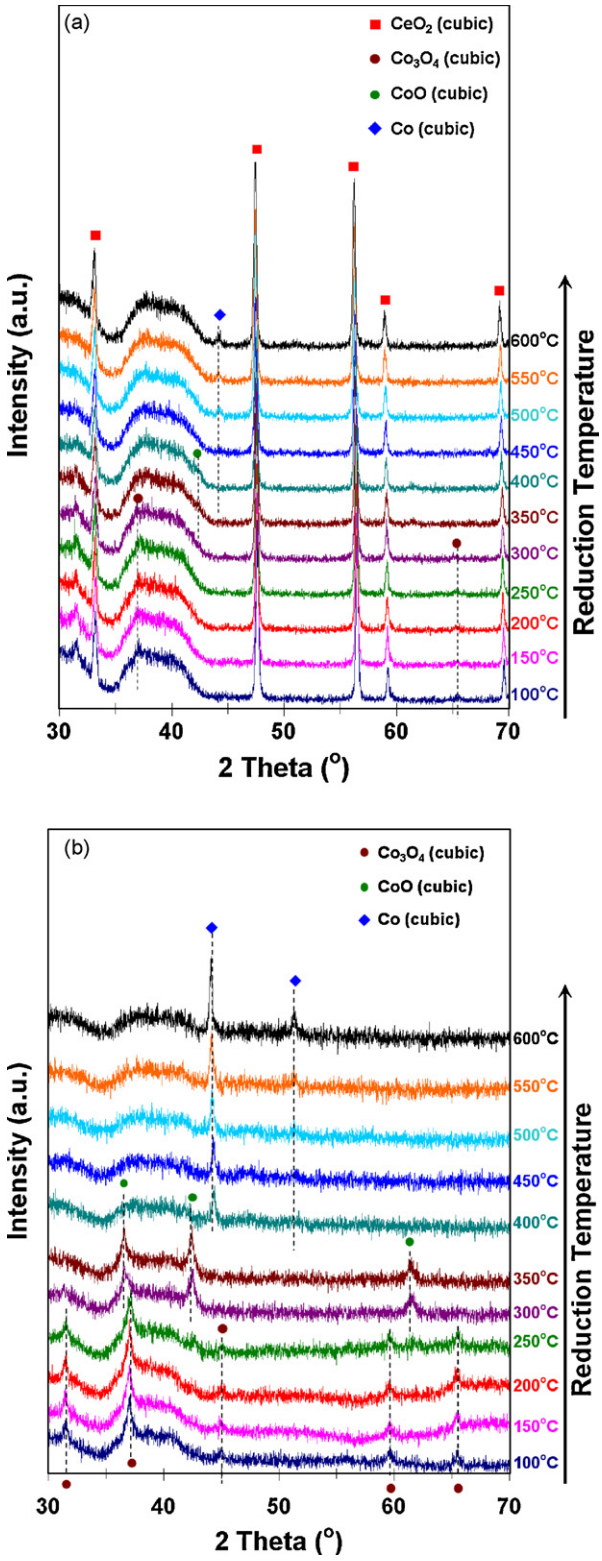

Fig. 6. *In situ* XRD patterns taken during reduction process over (a) Co/CeO_2(E) and (b) Co_3O_4.

The evolution of the crystalline phases during the reduction process over the calcined Co/CeO_2(E) is shown in the XRD patterns

Table 2
Cobalt/cobalt oxide crystal size estimation from XRD (nm).

Catalyst	Fresh[a]	Reduced[b]	Spent[c]
Co/CeO_2(A)	15	12	25
Co/CeO_2(E)	14	8	8

[a] Calculations are based on (3 1 1) diffraction line for Co_3O_4.
[b] Samples were reduced at 400 °C for 2 h. Calculations are based on (1 1 1) diffraction line for Co.
[c] XRD patterns were collected after time-on-stream for 40 h over 10%Co/CeO_2(E) and 10 h over 10%Co/CeO_2(A). Calculations are based on (1 1 1) diffraction line for Co.

Table 3
Surface elemental analysis using XPS technique over 10%Co/CeO_2(A) and 10%Co/CeO_2(E) after calcination and reduction.

	After calcination		After reduction	
	Co/CeO_2(A)	Co/CeO_2(E)	Co/CeO_2(A)	Co/CeO_2(E)
%Co	7.3	5.9	10.0	7.8
Co/Ce	0.27	0.43	0.25	0.34

acquired *in situ* (Fig. 6a). *In situ* XRD patterns obtained over bulk Co_3O_4 during a similar reduction process are also included (Fig. 6b) for comparison. The disappearance of the Co_3O_4 phase and the appearance of the CoO phase coincide at a reduction temperature of 350 °C. The diffraction line that corresponds to CoO phase disappears above 400 °C and a metallic Co phase appears at 450 °C, which is consistent with the TPR profile shown in Fig. 5. Compared to the standard Co_3O_4, the phase transformation takes place at a higher temperature, possibly due to the metal–support interaction. The crystal phase transformations during the reduction of Co/CeO_2(A) are also shifted to higher temperatures (data not shown) compared to the Co/CeO_2(E), sample, implying that this sample is more difficult to reduce, consistent with the TPR profiles shown earlier (Fig. 5).

Crystallite sizes of Co_3O_4 and metallic Co were determined using X-ray diffraction data. Table 2 summarizes the crystallite sizes for the two catalysts at different life stages calculated using Scherrer equation. The diffraction lines used for these calculations are (3 1 1) and (1 1 1) for the Co_3O_4 and Co phases, respectively. The fact that both of the samples have similar particle sizes for Co_3O_4 after calcination implies that the preparation in organic media has no effect on controlling the Co_3O_4 crystallite size. However, the crystallite sizes for the reduced and spent sample show a major difference, suggesting a strong effect of the impregnation medium in suppressing particle growth during reduction and reaction.

The reduction characteristics of the two samples prepared in organic versus aqueous media are compared through *in situ* LRS technique in Fig. 7a and b, respectively. The spectra corresponding to pure CeO_2, Co_3O_4 and CoO are also shown as reference. As the temperature is raised step-wise in a 5% H_2 stream, no significant phase transformation takes place below 400 °C. When the temperature is at 400 °C, Co/CeO_2(A) gives signal from both CO_3O_4 and CoO. When the temperature is raised up to 600 °C, cobalt oxide species are still visible in this sample. For the sample prepared in organic media, however, the reduction to metal takes place much more readily. At 450 °C, the bands that correspond to Co–O vibrations are no longer visible.

XPS surface analysis was performed over both samples at three different stages: (a) following calcination, (b) following reduction at 400 °C, and (c) following reduction at 600 °C. The spectra for Ce 3d and Co 2p regions are presented in Fig. 8 for Co/CeO_2(E). The oxidation state of Ce remains at +4 even in the sample that has been reduced at 600 °C, indicating that surface CeO_2 is not reduced within the tested reduction temperature range [31]. However, changes have been observed in the oxidation state of surface Co element. The presence of shake-up lines in the Co 2p XPS spectra of the sample reduced at 400 °C for 2 h points to the reduction of Co_3O_4 to CoO since the satellite peaks are characteristic of the Co^{2+} oxidation state [32–34]. The shoulder at 777.8 eV near the main

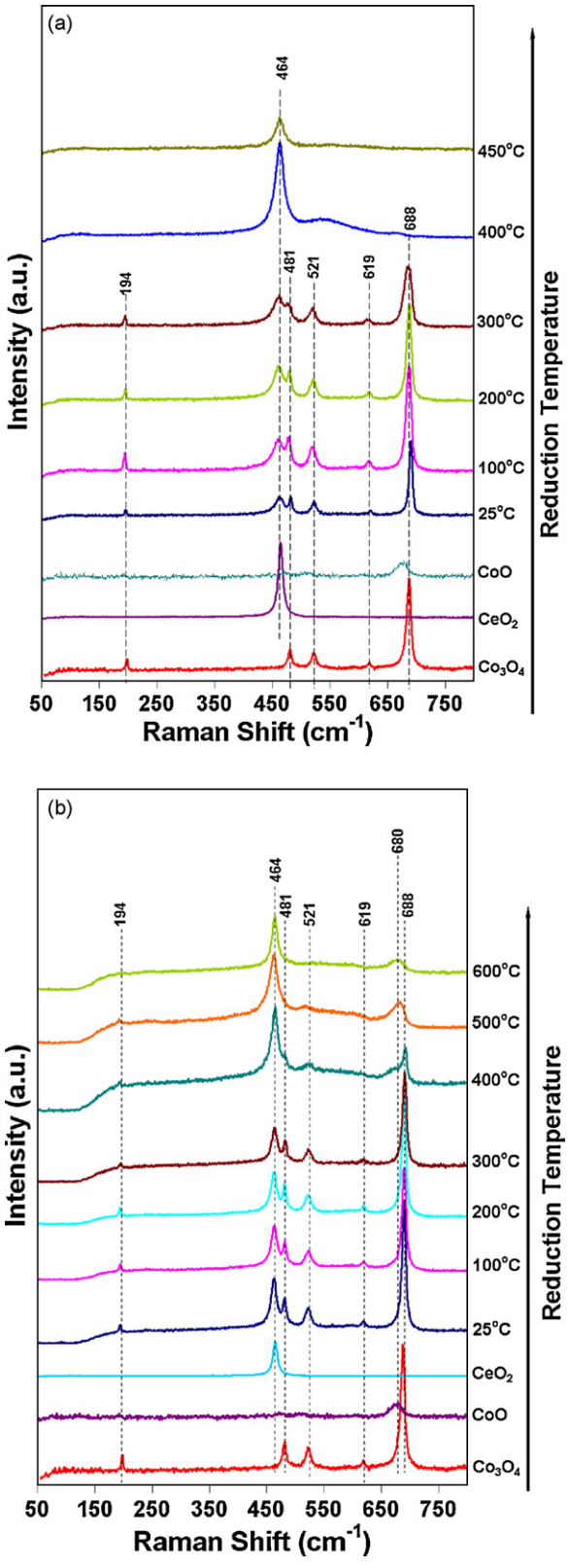

Fig. 7. *In situ* Raman spectra collected over (a) Co/CeO_2(E) and (b) Co/CeO_2(A) during reduction process.

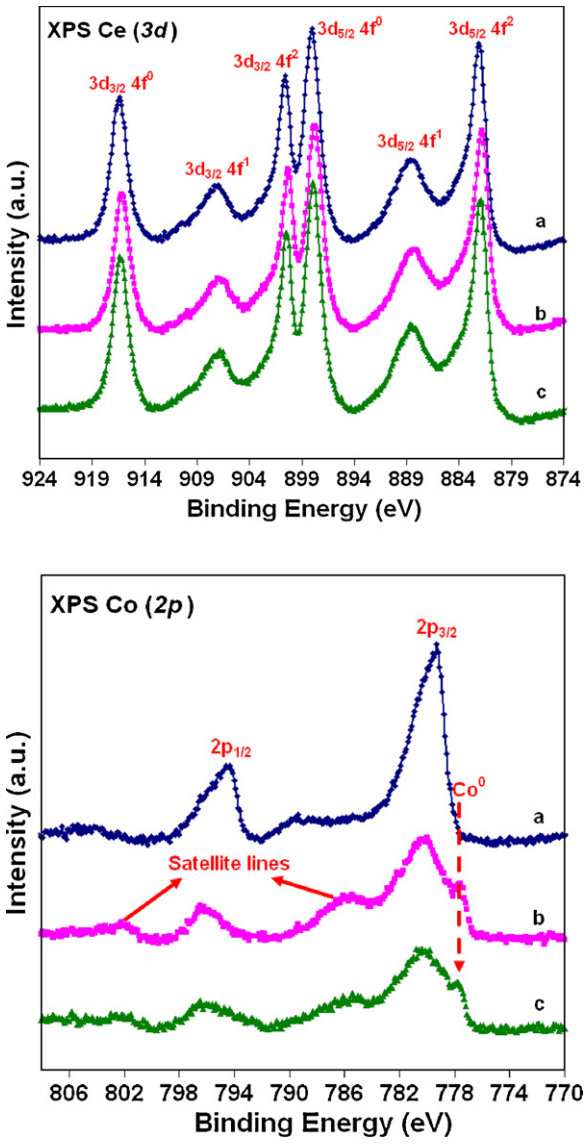

Fig. 8. The Ce (3d) and Co (2p) XPS spectra collected over Co/CeO_2(E) after (a) calcination at 450 °C for 3 h, (b) reduction at 400 °C for 2 h, and (c) reduction at 600 °C for 2 h.

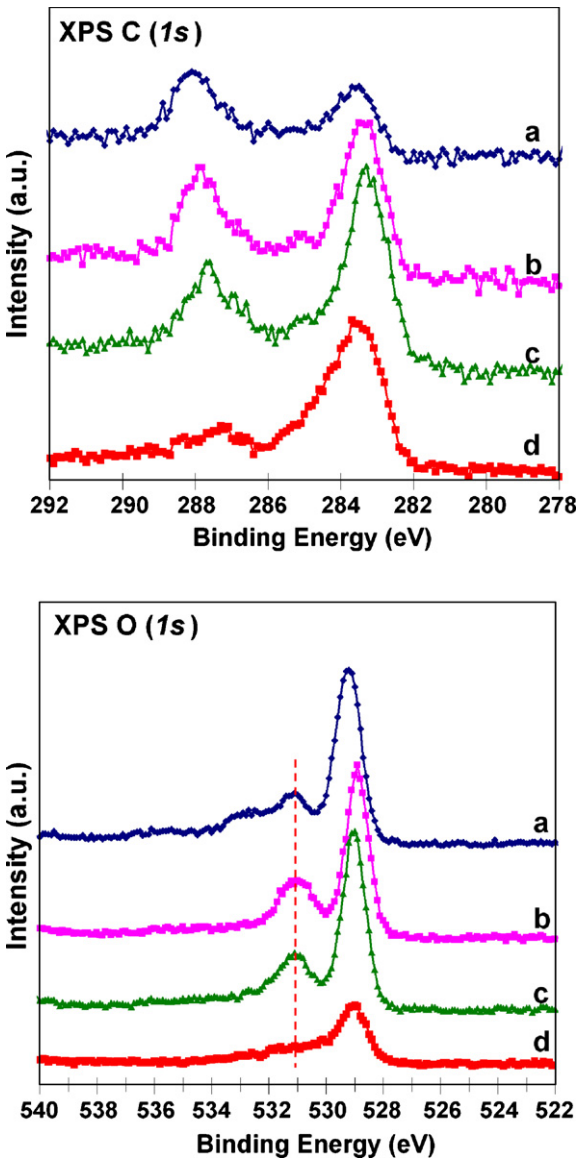

Fig. 9. The C (1s) and O (1s) XPS spectra collected over Co/CeO_2(E) after (a) calcination at 450 °C for 3 h, (b) reduction at 400 °C for 2 h, (c) reduction at 600 °C for 2 h, and (d) over Co/CeO_2(A) after calcination at 450 °C for 3 h.

peak at 780.2 eV shows the existence of metallic Co on the surface [35], implying that after the reduction treatment at 400 °C for 2 h, the Co_3O_4 particles have been reduced to a mixture of CoO and metallic Co. The spectrum taken following reduction at 600 °C shows a higher intensity for metallic Co signal, but Co^{2+} signal is still present. Although at 600 °C, reduction of the cobalt oxide phase to metallic Co is expected to be complete, presence of Co-oxide species can be due to partial reoxidation of the surface by lattice oxygen from the support. The oxygen mobility in CeO_2 has been demonstrated before in several different systems [16,36,37].

In order to evaluate the surface concentrations of the Co and Ce elements before and after reduction and compare this ratio between the two catalysts evaluated, the Co/Ce atomic ratios determined by XPS results have been quantified and tabulated in Table 3. As can be seen, the Co/CeO_2(E) has significantly higher Co/Ce ratio than its counterpart both before and after reduction, indicating better cobalt dispersion over Co/CeO_2(E), which is consistent with H_2 chemisorption results, which showed 9.4% and 15.1% Co dispersion for Co/CeO_2(A) and Co/CeO_2(E), respectively. In addition, it is worth noting that although Co concentration on the surface decreases for both of the catalysts following reduction, the % decrease is larger for the Co/CeO_2(A) sample, suggesting a sintering effect during reduction over this catalyst. The reduction temperature did not affect much the Co concentration on the surface of the Co/CeO_2(E) when it was reduced at 600 °C. There was no additional decrease in the Co surface concentration over this catalyst compared to what was obtained following the lower temperature reduction process.

The XPS spectra taken over the Co/CeO_2(A) (data not shown) exhibited features similar to those of Co/CeO_2(E). When the C 1s and O 1s regions of the spectra were compared, however, the two catalysts showed major differences (Fig. 9). C 1s spectrum showed a feature at a binding energy of 287.8 eV over the Co/CeO_2(E) catalyst. This peak was observed in all three spectra, the one taken over the fully oxidized sample as well as the ones taken following reduction at 400 and 600 °C. Although a weak peak also appeared around 287 eV over the Co/CeO_2(A) sample, it was much weaker and close to 1 eV apart. When O 1s spectra were compared, the Co/CeO_2(E) catalyst showed a peak at 531.1 eV, which remained even after reduction at 600 °C. This peak was absent in the O 1s spectrum taken over the sample prepared in aqueous media. Appearance of

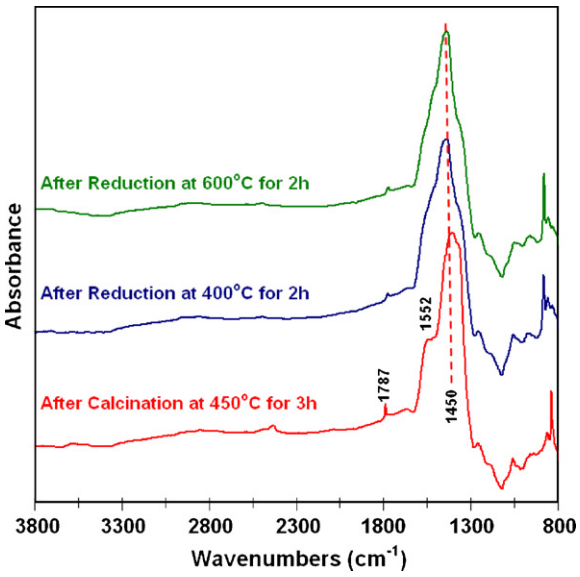

Fig. 10. DRIFTS spectra of $Co/CeO_2(E)$ at various life stages.

these additional peaks in the O 1s and C 1s spectra suggests the presence of some oxygenated carbon species on the surface of the catalyst prepared in organic media [35]. It should be noted that the presence of a shoulder at 533.5 eV in O 1s spectrum over the fully oxidized sample and the noticeable change in the relative intensities of the C 1s peaks suggest that these species go through some transformation during the reduction steps, but are stable enough to remain on the surface even when exposed to a high-temperature reducing atmosphere.

The presence of oxygenated carbonaceous species was further verified by the DRIFTS experiments performed over the samples prepared in different media. Fig. 10 shows the difference spectra plotted by subtracting the spectrum collected over the sample prepared in aqueous media from the ones taken over the $Co/CeO_2(E)$ sample, following three different pre-treatment steps. The band located at 1787 cm^{-1} suggests the presence of a carbonyl group (ν(C=O)), possibly in a carboxylate species. However, this band is much weaker compared to the ones located at 1552 and 1450 cm^{-1}. The presence of these bands together with a weaker one around 880 cm^{-1}, suggests an acetate species, possibly coordinated to a metal center. Formation of acetate species has been identified as the preferred reaction pathway in ethanol steam reforming for high H_2 selectivity, as reported in our previous publications [16,29]. Based on our *in situ* DRIFTS experiments, the acetate species evolves from the ethoxide species originating from the dissociative adsorption of ethanol. The acetate species formed will subsequently be oxidized to carbonate and finally decomposed to CO_2.

Although there are slight shifts in the band position when the samples are reduced, the main features of the spectra remain the same. Although it is difficult to make definitive assignments due to large number of overlapping bands of this region, it appears that there are oxygenated carbonaceous species on the surface and these species are stable enough to withstand calcination and reduction steps, the latter at temperatures even as high as 600 °C.

The observation that the presence of such species over the (E) sample is the only apparent difference between the two catalysts suggests that these oxygenated carbon species may be playing a role in the superior performance of the catalysts prepared in organic media. One possibility is that the presence of these organic ligands may keep the Co particles segregated, ensuring a high level of dispersion throughout their life history. The other possibility is that these species may be blocking the sites that lead to the dehydration and aldol condensation-type reactions, which would lead to coking and acetone formation, respectively. A related possibility is that the presence of acetate species on the surface of the catalysts prior to any reactions may make it easier for ethanol to be converted to surface acetate species, by following an "imprint" left on the surface during the impregnation step. The concept of molecular imprinting on metal complexes has been previously reported in different studies [38–42] and many of these studies have been summarized in a review article by Tada and Iwasawa [43]. In these studies, usually ligands are used as template molecules, which, when removed, leave behind cavities near the metal site. One of the possible mechanisms through which such imprinting can help is by providing "shape-selective reaction space on the active metal center" [38]. It is conceivable that what is observed in our study stems from such a phenomenon where the acetate-type surface species formed during the impregnation step may provide necessary surface geometry for the selective reaction pathway in ethanol steam reforming. However, the current results do not provide sufficient evidence to prove or to refute any of these aforementioned possibilities.

4. Conclusions

The $Co–CeO_2$ catalysts prepared in ethanol medium showed significant improvement in catalytic performance (higher H_2 yield, higher stability and fewer side reactions) compared to the ones prepared in aqueous media. Characterization results showed the presence of oxygenated carbon species, possibly metal-coordinated acetates, on the surface. These species are likely to play a role in the improved performance. Although the nature of this role is not clear at this point, possibilities include a segregation effect that prevents sintering, a site-blocking effect that suppresses the side reactions, or an "imprinting" effect that makes it easier for the acetate intermediates to form on the surface. Additional studies are needed to elucidate the exact role played by these surface species resulting from the impregnation medium.

Acknowledgement

We gratefully acknowledge the funding from the U.S. Department of Energy through the grant DE-FG36-05GO15033.

References

[1] J.P. Breen, R. Burch, H.M. Coleman, Appl. Catal. B: Environ. 39 (2002) 65–74.
[2] D.K. Liguras, D.I. Kondarides, X.E. Verykios, Appl. Catal. B: Environ. 43 (2003) 345–354.
[3] J.R. Salge, G.A. Deluga, L.D. Schmidt, J. Catal. 235 (2005) 69–78.
[4] V. Fierro, O. Akdim, C. Mirodatos, Green Chem. 5 (2003) 20–24.
[5] A. Haryanto, S. Fernando, N. Murali, S. Adhikari, Energy Fuels 19 (2005) 2098–2106.
[6] P.D. Vaidya, A.E. Rodrigues, Chem. Eng. J. 117 (2006) 39–49.
[7] S. Cavallaro, V. Chiodo, S. Freni, N. Mondello, F. Frusteri, Appl. Catal. A: Gen. 249 (2003) 119–128.
[8] C. Diagne, H. Idriss, A. Kiennemann, Catal. Commun. 3 (2002) 565–571.
[9] S. Cavallaro, Energy Fuels 14 (2000) 1195–1199.
[10] J.R. Mielenz, Curr. Opin. Microbiol. 4 (2001) 324–329.
[11] J. Llorca, P.R. de la Piscina, J.-A. Dalmon, J. Sales, N. Homs, Appl. Catal. B: Environ. 43 (2003) 355–369.
[12] J. Llorca, N. Homs, J. Sales, P.R. de la Piscina, J. Catal. 209 (2002) 306–317.
[13] A. Yee, S.J. Morrison, H. Idriss, J. Catal. 186 (1999) 279–295.
[14] L.V. Mattos, F.B. Noronha, J. Catal. 233 (2005) 453–463.
[15] N. Laosiripojana, S. Assabumrungrat, Appl. Catal. B: Environ. 66 (2006) 29–39.
[16] H. Song, U.S. Ozkan, J. Catal. 261 (2009) 66–74.
[17] N. Homs, J. Llorca, P.R. Piscina, Catal. Today 116 (2006) 361–366.
[18] A.E. Galetti, M.I.F. Gomez, L.A. Arrua, A.J. Marchi, M.C. Abello, Catal. Commun. 9 (2008) 1201–1208.
[19] J. Llorca, N. Homs, J. Sales, J.G. Fierro, P.R. Piscina, J. Catal. 222 (2004) 470–480.
[20] F. Haga, T. Nakajima, H. Miya, S. Mishima, React. Kinet. Catal. Lett. 63 (1998) 253–259.
[21] J. Llorca, P.R. Piscina, J. Dalmon, J. Sales, N. Homs, Appl. Catal. B: Environ. 43 (2003) 355–369.
[22] J. Panpranot, S. Kaewkun, P. Praserthdam, J.G. Goodwin, Catal. Lett. 91 (2003) 95–102.

[23] H. Song, L. Zhang, U.S. Ozkan, Green Chem. 9 (2007) 686–694.
[24] D.I. Enache, B. Rebours, M.R. Auberger, R. Revel, J. Catal. 205 (2002) 346–353.
[25] E. Ruckenstein, H.Y. Wang, Catal. Lett. 70 (2000) 15–21.
[26] M.S. Batista, R.K.S. Santos, E.M. Assaf, J.M. Assaf, E.A. Ticianelli, J. Power Sources 124 (2003) 99–103.
[27] S. Song, A.J. Akande, R.O. Idem, N. Mahinpey, Eng. Appl. Artif. Intel. 20 (2007) 261–271.
[28] S. Ho, Y. Su, J. Catal. 168 (1997) 51–59.
[29] H. Song, L. Zhang, U.S. Ozkan, Catal. Today 129 (2007) 346–354.
[30] B. Jongsomjit, J. Panpranot, J.G. Goodwin, J. Catal. 215 (2003) 66–77.
[31] J. Kugai, V. Subramani, C. Song, M.H. Engelhard, Y.H. Chin, J. Catal. 238 (2006) 430–440.
[32] L.F. Liotta, G.D. Carlo, G. Pantaleo, A.M. Venezia, G. Deganello, Appl. Catal. B: Environ. 66 (2006) 217–227.
[33] M. Haneda, Y. Kintaichi, N. Bion, H. Hamada, Appl. Catal. B: Environ. 46 (2003) 473–482.
[34] F.B. Noronha, C.A. Perez, M. Schmal, R. Frety, Phys. Chem. Chem. Phys. 1 (1999) 2861–2867.
[35] H. Idriss, C. Diagne, J.P. Hindermann, A. Kiennemann, M.A. Barteau, J. Catal. 155 (1995) 219–237.
[36] L.F. Liotta, M. Ousmane, G. Di Carlo, G. Pantaleo, G. Deganello, G. Marci, L. Retailleau, A. Giroir-Fendler, Appl. Catal. A: Gen. 347 (2008) 81–88.
[37] T.G. Kuznetsova, V.A. Sadykov, Kinet. Catal. 49 (2008) 840–858.
[38] M Tada, Y. Iwasawa, Coordin. Chem. Rev. 251 (2007) 2702–2716.
[39] M. Tada, T. Sasaki, Y. Iwasawa, J. Phys. Chem. B 108 (2004) 2918–2930.
[40] M. Tada, Y. Iwasawa, J. Mol. Catal. A 204 (2003) 27–53.
[41] M. Tada, T. Sasaki, Y. Iwasawa, Phys. Chem. Chem. Phys. 4 (2002) 4561–4574.
[42] M. Tada, T. Sasaki, Y. Iwasawa, J. Catal. 211 (2002) 496–510.
[43] M. Tada, Y. Iwasawa, J. Mol. Catal. A 199 (2003) 115–137.